COBEM UBERLÂNDIA 2019

ABCM Associação Brasileira de Engenharia e Ciências Mecânicas

25th ABCM International Congress of Mechanical Engineering
October 20-25, 2019, Uberlândia, MG, Brazil

CHARACTERIZATION OF WIND TURBINE BLADE AERODYNAMICS PARAMETERS USING LARGE EDDY SIMULATION WITH AN IMMERSED BOUNDARY METHOD

Leandro José Lemes Stival
Federal University of Parana, Curitiba, Parana, Brazil
leandro.stival@ufpr.br

João Marcelo Vedovoto
Federal University of Uberlandia, Uberlandia, Minas Gerais, Brazil
vedovoto@ufu.br

Fernando Oliveira de Andrade
Federal Technology University of Parana, Curitiba, Parana, Brazil
fandrade@utfpr.edu.br

Abstract. *The demand for energy has been increasing in the last decade due to the global economic growth. Wind energy has offered a range of advantages, as a technology already developed along with a prospection on the market. A comprehensive assessment of wind resources is required to absorb the entire gain of wind power. Thus, the main goal of this work is to test how large eddy simulation (LES) alongside immersed boundary method (IB) behaviors, in order to characterize the most important parameters experimental wind turbine blade aerodynamics. The LES method is responsible for the solution of the filtered proprieties related to the flow field over the eulerian referential, while the IB method solves the problems related to fluid-structure interaction, where the forces are assessed at the solid-fluid interface, which corresponds to the lagrangian formulation. The experimental wind turbine blade utilized was the NREL S809. The drag and lift coefficients results showed good agreement in comparison to the experimental data as a function of different angles of attack. The drag coefficient itself presented excellent results. The downstream wake centerline velocity recovery analysis for different angles of attack presented a quick recovery for small angles of attack. However, for greater angles of attack, the recovery almost reached 100% of the free stream wind speed at the end of the domain for a couple of angles. The vorticity analysis presented bigger eddies structures for higher angles of attack as expected.*

Keywords: *Large eddy simulation, immersed boundary, wind turbine.*

1. INTRODUCTION

The demand for energy has been increasing in the last decade due to the global economic growth. Such development has risen quickly over the past three decades. Although, the consumption of fossil fuels has become a point of environmental concern (Zhong *et al.*, 2017). Increasing energy consumption not only results in depletion of energy resources, but also gives rise to problems like global warming and greenhouse effect through emissions generated by burning of fossil fuels (Edelenbosch *et al.*, 2017). As a result of that, some countries were driven to prospect and adjust to renewable resources to maintain the expanding energy requirement (Lund, 2007; Şiir Kılkış *et al.*, 2018).

Therefore, the development of several sources of renewable energies, such as solar, hydropower and wind energy is extremely important and timely. Amid these renewable resources, wind energy has offered a range of advantages, as a technology already developed along with a prospection on the market (Leung and Yang, 2012).

Wind turbines convert the kinetic energy of the flow that passes the swept area of the wind turbine to mechanical torque on the rotor hub. The electromagnetic conversion transforms the torque into electrical energy with the assistance of an electric generator. However, according to Betz's theory, the maximum value of efficiency that a wind turbine can reach is 59.3%, as the wind speed reduces when approaches the rotor plane (Çengel, 2010). Although, it is important to point out that the efficiency of the wind turbines installed nowadays presents average values around 30%.

Therefore, attending to study and project large wind farms layouts, wind turbine modelling is a crucial element of the energy yield. Aiming to diminish power losses, it is essential to have a valuable understanding of the behavior of wakes in wind power plants. Such knowledge can be obtained by modelling the wake effects in wind turbines (Mo *et al.*, 2013; Vermeer *et al.*, 2003; Tsalicoglou, 2012). A comprehensive assessment of wind resources is required to absorb the entire gain of wind power (Rehman and Al-Abbadi, 2005; Wharton and Lundquist, 2012). Thus, the main goal of this study

is to test how large eddy simulation alongside immersed boundary method behaviours in order to characterize important parameters related to a small wind turbine aerodynamics, being characterized by its NREL S809 blade.

2. METHODOLOGY

This work aims to present a new approach to model and simulate the flow around wind turbines. A first approach at the partial differential equations governing fluid flows, which corresponds to solve the Navier Stokes equations through a hybrid modelling methodology, which applies the coupling of Large Eddy Simulation (LES) and Immersed Boundary Method (IB). The LES method is responsible for the solution of the filtered proprieties related to the flow field over the eulerian referential, while the IB method solves the problems related to fluid-structure interaction, where the forces are assessed at the solid-fluid interface, which corresponds to the lagrangian formulation.

2.1 Governing Equations

This section presents the eulerian mathematical formulation, which corresponds to the governing equation for the continuous fluid domain, approaching the momentum and continuity equations.

In the eulerian formulation applied consists of a unique fluid inside the control volume, then mass balance and momentum balance equations can be written as:

$$\frac{\partial(\rho)}{\partial t} + \frac{\partial(\rho u_i)}{\partial x_i} = 0, \tag{1}$$

$$\frac{\partial(\rho u_i)}{\partial t} + \frac{\partial(\rho u_i u_j)}{\partial x_j} = -\frac{\partial p}{\partial x_i} + \frac{\partial(\tau_{ij})}{\partial x_j} + f_i, \tag{2}$$

where p is pressure, ρ is the fluid density, u_i is the velocity vector component at i, τ_{ij} represents the molecular viscous stress and f_i is the component i of the source term, where into the immersed boundary methodology is the vector of the eulerian force field, which means the representation of a complex geometry inside of the flow.

Moreover assuming that is a newtonian fluid, and since μ is the kinematic viscosity of the fluid. The stress can be modeled as the Stokes viscosity stress, representing as follows:

$$\tau_{ij} = \mu\left(\frac{\partial u_i}{\partial x_j} + \frac{\partial u_j}{\partial x_i}\right) - \frac{2}{3}\mu\delta_{ij}. \tag{3}$$

Then assuming an incompressible flow due to any heat transference consideration in the air flow, considering Mach number lower than 0.3. Snel (2003) and Sanderse (2009) confirm the incompressibility assumption for wind power application, mainly based on the lower velocities in the wake region to justify. Therefore, the incompressibility continuity and momentum equations become:

$$\frac{\partial(u_i)}{\partial x_i} = 0, \tag{4}$$

$$\frac{\partial(u_i)}{\partial t} + \frac{\partial(u_i u_j)}{\partial x_j} = -\frac{1}{\rho}\frac{\partial p}{\partial x_i} + \frac{\partial}{\partial x_j}\left[\nu\left(\frac{\partial u_i}{\partial x_j} + \frac{\partial u_j}{\partial x_i}\right)\right] + f_i. \tag{5}$$

2.2 Large Eddy Simulation

A complete solution for the system that includes the governing equations, considering that for high Reynolds Number the computational effort is quite large because the order of magnitude of temporal and spatial scales to represent all scales in the flow.

Therefore, the flow over a wind power plant may range eddies from the boundary layer of the blades to a length that comprises many wind turbines (Mehta *et al.*, 2014). As a choice, the Large Eddy Simulation (LES) is a technique that allows to model particular eddies, in order to reduce the degrees of freedom, which means removing certain information over the flow. Then resolving the remain structures with the filtered Navier Stokes equations.

However, the LES method consists of a spatial filter in the transport equations, which enables to select the large eddies of the flow to be calculated. Meanwhile, the sub-grid scale (SGS) models the smaller eddies, which are smaller than

the grid. In the filtered Navier-Stokes equations, there is a dissociation of the generic signal $f(\vec{x},t)$ into two parts, one characterizes the filtered part $\bar{f}(\vec{x},t)$ while $f'(\vec{x},t)$ represents the fluctuation part, as follows:

$$f(\vec{x},t) = \bar{f}(\vec{x},t) + f'(\vec{x},t). \tag{6}$$

Moreover, the filtered part can be expressed as:

$$\bar{f}(\vec{x},t) = \int_D f(\vec{x}',t)\, G(\vec{x}-\vec{x}')\, d\vec{x}'. \tag{7}$$

Therefore, considering the mass balance exposed in the Eq. (4) and applying the filtering over this equation, assuming the cumulative property over both operators, it is possible to obtain the mass balance for the filtered velocities:

$$\frac{\partial(\bar{u}_i)}{\partial x_i} = 0. \tag{8}$$

In the analog way of the above process is possible to represent the momentum equation. Applying the filter over the Eq. (5) and mathematically manipulating using the properties in order to obtain the filtered momentum equation. Although, in the nonlinear term there is a filtered multiplication turning it not possible to solve this equation at this form, in order to reach the multiplication of the filtered variables it is important to define the global sub-grid stress of the turbulence:

$$\frac{\partial(\bar{u}_i)}{\partial t} + \frac{\partial(\bar{u}_i\bar{u}_j)}{\partial x_j} = -\frac{1}{\rho}\frac{\partial \bar{p}}{\partial x_i} + \frac{\partial}{\partial x_j}\left[\nu\left(\frac{\partial \bar{u}_i}{\partial x_j} + \frac{\partial \bar{u}_j}{\partial x_i}\right) - \tau_{ij}\right]. \tag{9}$$

2.3 Immersed Boundary Method

The immersed boundary method applies an independent grid to define the body inside the fluid flow. The main advantage of this model is to simulate the flows over complex geometries applying a cartesian grid to the fluid or eulerian domain. The formulation proposed in Wang *et al.* (2008) is applied at this work, which utilizes the multi-direct forcing method.

The force term, f_i, in the momentum equation controls the definition of the immersed boundaries. In order to calculate this force is commonly utilized a distribution function:

$$f_i(\vec{x}) = \sum_K \vec{F}(\vec{x}_K)\, D_{ij}(\vec{x}-\vec{x}_K)\, \Delta V(\vec{x}_K), \tag{10}$$

where $\vec{x}$ is the eulerian volume coordinate, $\vec{x}_K$ is the langrangian element coordinate, $\Delta V(\vec{x}_K)$ the volume of the lagrangian element e D_{ij} represents the distribution function. This work applies the hat function, which presents the following formulation, where Δ is the characteristic length of the eulerian grid:

$$D_{ij}(\vec{x}) = g(\vec{x}_K - \vec{x})\, g(\vec{y}_K - \vec{y})\, g(\vec{z}_K - \vec{z}). \tag{11}$$

$$g(r) = \begin{cases} \frac{1-\|r\|/\Delta}{\Delta} & , \|r\| \le \Delta \\ 0 & , \|r\| > \Delta. \end{cases} \tag{12}$$

This function presents an important characteristic, when the eulerian volumes are far from the lagrangian points, lower is the force value distributed at those points. Besides that, a crucial property of it relates the integration along all the domain, which obtains a unitary value. This is due to the conservative distribution process of the function (Mittal and Iaccarino, 2005). Therefore, $\vec{F}(\vec{x}_K)$ stands for the force at lagrangian point, which will be distributed over the eulerian field to delimit the boundary. Moreover, the momentum equation still valid in each of the lagrangian points. Regarding the continuous hypothesis, which those points compose the eulerian domain as well (da Silva Melo, 2012).

3. LES-IB COUPLING

As seen in the sections before, the mathematical formulation that involved the LES and IB methods based on different referential, which are applied at this work. The first approach correlates the eulerian coordinate system while the second one brings the lagrangian perspective of the immersed body distributed over the flow.

|For the eulerian referential, the momentum and mass balance equations provide the filtered velocity and pressure fields. However, the velocity field u^* and position x_i provided from eulerian referential are transferred to lagrangian points, in order to calculate the velocity of the body movement at the lagrangian points U_i^*, after that calculates the force F_i at those points. Later, this force is also distributed over the eulerian domain, and the cycle continues iteratively for the subsequent time step, where the convergence criteria relates the minimum residual established for the case.

In order to contemplate the established objectives of the study, the Navier-Stokes equations were discretized and implemented in the so called AMR3D code. Code developed in the MFlab of the Federal University of Uberlandia, which applies a block-structured adaptive mesh refinement.

4. RESULTS AND DISCUSSION

In the last decades, experimental studies have been elaborated in wind tunnel tests. Ramsay *et al.* (1995); Hand *et al.* (2001); Simms *et al.* (2001) performed tests that may be considered the most precise and efficient approach to characterize the forces acting over wind turbine blades. These authors developed a structural model and verification procedures for the wind experimental Phase VI of the National Renewable Energy Laboratory (NREL), which is a two-bladed wind turbine, as depicted in Fig. 1. The wind speeds varied from 5 m/s to 25 m/s at a hub height of 12.2 m and a rotor diameter of 10.058 m. The experiments performed a diverse number of aerodynamic measurements and a great amount of structural information to develop a fluid-structural model.

Figure 1: Two Bladed wind turbine from experimental Phase VI of the National Renewable Energy Laboratory (NREL). Source:Hand *et al.* (2001)

Figure 2 represents the developed blade to represent the experimental NREL S809, following the airfoil characteristics and patterns, where Fig. 2(a) depicts the frontal view of the blade, characterizing the height of the blade. Figure 2(b) shows the perspectives of the variation in terms of the chord length of the blade and Figure 2(c) presents the airfoil characteristics and the twisted angles applied.

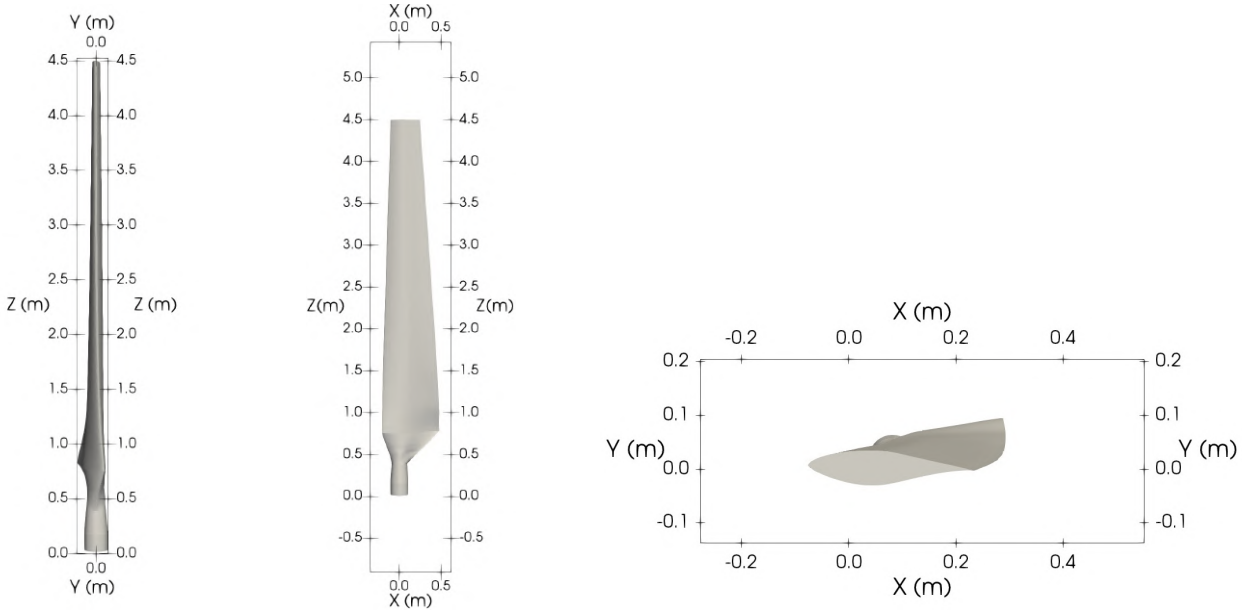

(a) Frontal view (b) Lateral view (c) Top view

Figure 2: NREL S809 (a) frontal, (b) lateral and (c) top view.

The NREL S809 blade was constructed in the CATIA software and meshed in the ICEM CFD software. The blade mesh what represents the lagrangian domain contains 80730 cells, the Fig. 3 shows the color map of the blade in terms of the area distribution for each mesh cell, presenting the variation of the area at each cell.

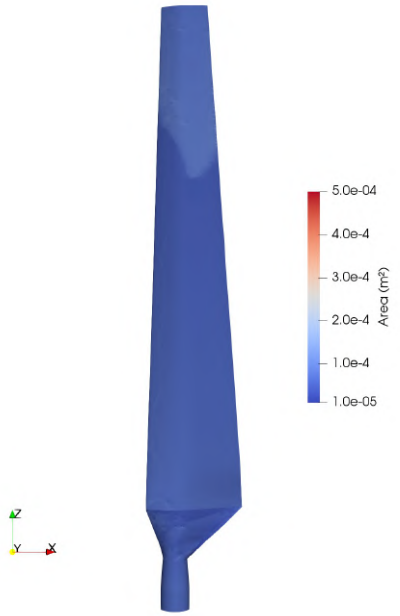

Figure 3: Mesh area of the NREL S809 Blade

The eulerian domain of the flow is set to 30 m in the x-direction, 10 m in the y-direction and also 10 m in the z-direction. The XZ-plane is presented in the Fig. 4, which represents the computational grid of the eulerian mesh. The initial mesh refinement is set up with 24 x 8 x 8 volumes for the coarser grid (base level) in the xyz directions, respectively. Then characterizing the number of physical levels equals to 7, which means that there is a 7 time refinement since the base level. This finest grid level is always around the blade shape.

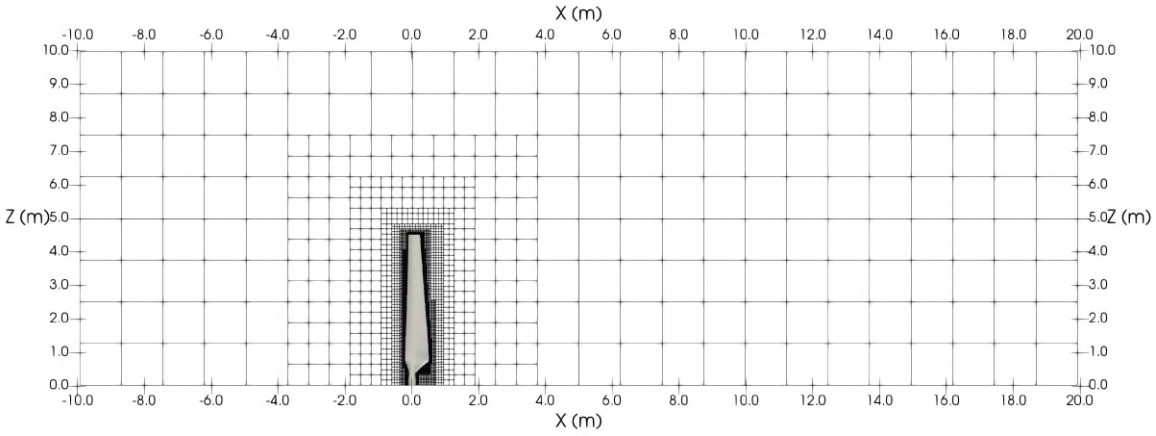

Figure 4: Eulerian mesh of the flow

All the simulations that have been made utilized the adaptive mesh refinement, with parallel processing, where the domain was divided into 8 processes. The mesh refinement criteria were lagrangian points and vorticity, where a non-dimensional number is calculated following Barbi (2016):

$$\frac{\|\omega\|\,\Delta}{u_{max}} \geq \zeta, \tag{13}$$

where ω is the vorticity magnitude, Δ is the grid length, u_{max} is the velocity magnitude and ζ is a constant, which states that as bigger its values more sensible to the refinement is the region, therefore for this article it was applied $\zeta = 0.08$.

For this study of the flow around a NREL S809 in the AMR3D code, an imposed velocity condition was employed in the inflow (u =10 m/s), characterizing a Dirichlet type of boundary condition. The lateral planes (XZ-planes) were

characterized as symmetry, this condition was applied as well in the top plane (XY-plane). The bottom plane (XY-plane) sets a free-slip condition in order to represent an enchased blade coupled with the rotor. A Neumann boundary condition was applied for pressure. The initial conditions for velocities were u=10, v=0 and w=0 m/s while the pressure was set to 0 Pa. In these simulations, the fluid properties are ρ=1.225 kg/m, μ=0.0000182 kg/(m s) and setting a Reynolds number ($Re \approx 300.000$). The final simulation time was 60 physical seconds.

4.1 Drag and Lift Coefficients

In order to perform simulations and compare with experimental data from NREL Hand *et al.* (2001). The following considerations took the averaged integral lift and drag coefficients obtained from different angles of attack, varying from 10 to 45°, by 5°increments. The velocity approaches the free wind velocity at 10 m/s. Figure 5 presents the lift coefficient and the drag coefficients as a function of the angle of attack of the chosen blade, NREL S809, in comparison to the experimental data provided by NREL.

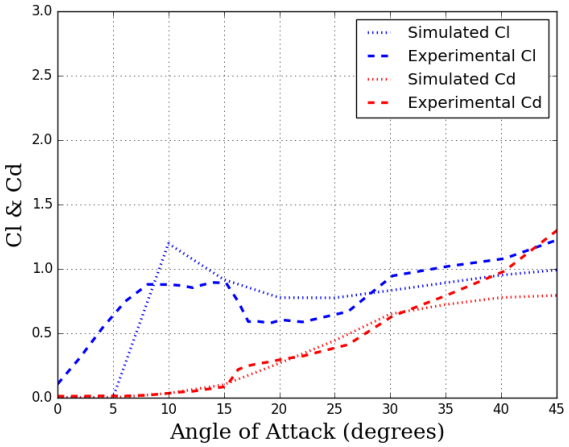

Figure 5: Lift and Drag coefficients

It is noticeable that the drag coefficient obtained better agreement with the experimental data than the lift coefficient. This might be justified by the higher increment of 5°of angles of attack for the simulations, for the future research development will be created shorter angle increments, every 1 or 2 °. Although, the lift coefficient simulated presents the same pattern as the experimental one in terms of the evolution of the angles of attack. There is a fast increasing until 10 to 15°followed by a decreasement until 30°and then a small rate recovery from that. In terms of drag coefficient, the only disparity occurs after 35°of angle of attack. Therefore, it is important to have small variation degrees for angles of attack over the following steps of the study.

Figure 6 shows the aerodynamic relation of lift coefficient over drag coefficient (C_l/C_d) as a function of different angles of attack. This relation is important in order to determine the performance and efficiency of an airfoil at a particular angle of attack. However, the shape of an airfoil affects the production of lift which will vary with changes in the angle of attack.

The lift curve shows a steady increase in the coefficient of lift with an increase in the angle of attack, up to the stall angle of attack. However, a blade has its best lifting ability closer to the stalling angle of attack. Regrettably, near the stalling angle, the blade also develops moderate drag.

5. Flow Field Analysis

For a detailed comparison of the flow field velocities, wind speed profiles are plotted and analyzed in the streamwise direction. The flow field velocities characteristics are shown in $x-y$ graphical format, in which the vertical axis represents the freestream velocity recovery (also named as velocity deficit). The horizontal axis shows the downstream distance behind the wind turbine in the wake, centerline longitudinal analysis and cross-sectional at $X = 1D$, where D is the NREL S809 diameter.

The streamwise wind speed along the wake centerline for different angles of attack are presented in Fig. 7, 10°to 25°, and Fig. 8, 30°to 45°, respectively. Figure 7 clearly shows the high extract energy in the near wake downstream the NREL S809, where the velocity recovery reaches a minimum value range around 0 to 0.5 m/s right after the blade. After $1D$ downstream distance, the velocity recovery increases up to 70% of the free stream wind speed. Achieving 85% to 90% recovery at the end of the domain.

Meanwhile, Fig. 8 also presents a high extract energy characteristics right after the NREL blade. Just at downstream

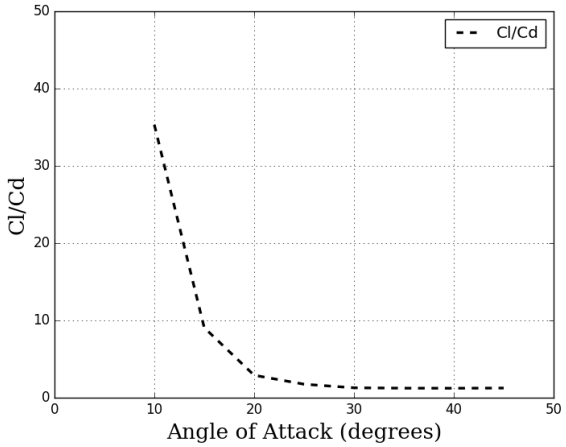

Figure 6: Cl/Cd ratio

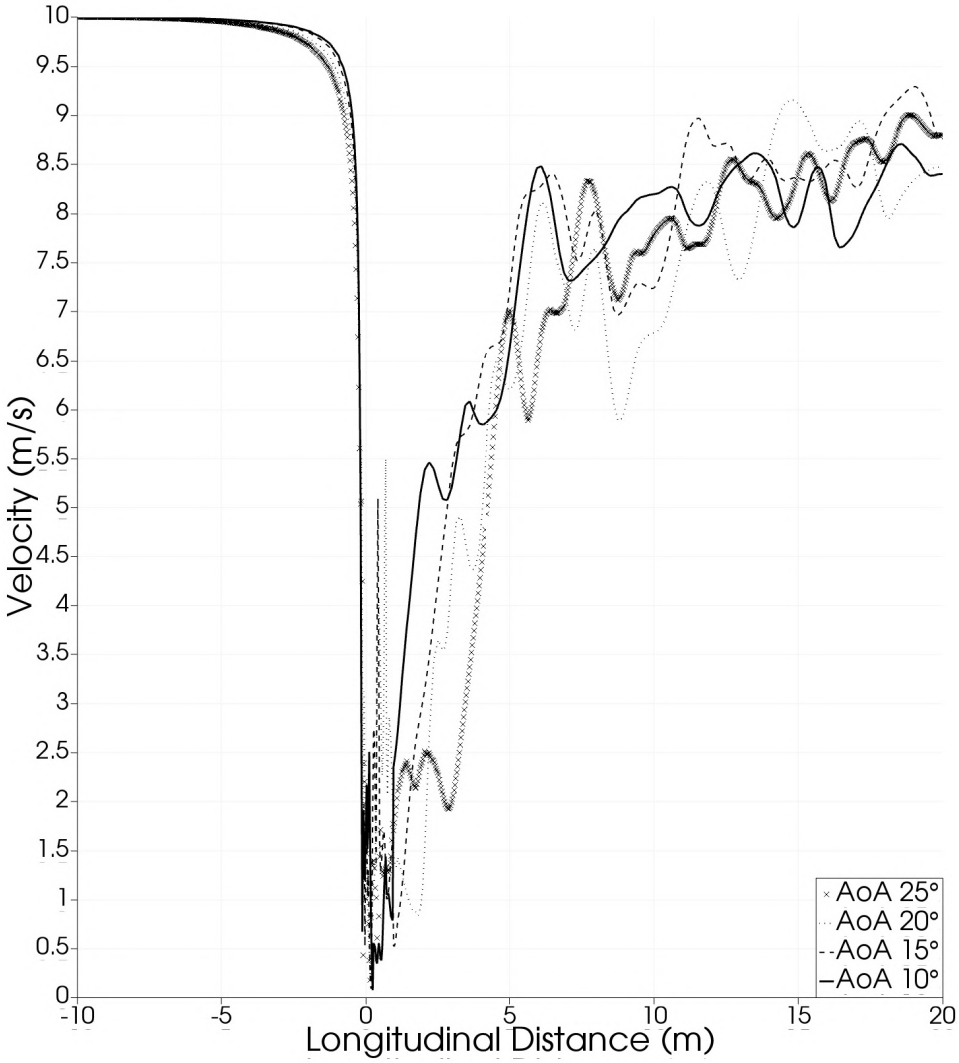

Figure 7: Longitudinal velocity recovery for different angles of attack from 10°to 25°

of the blade the wind speed reaches values close to zero, then the velocity has rapid recovery up to 65% at $1D$ downstream distance. The velocity recovery increases in a shorter rate up to the end of the flow domain, getting close to 100% recovery for a couple of cases.

Figure 9 compares the vorticity snapshots in the XY-plane for four different angles of attack, 10°, 20°, 30°and 40°,

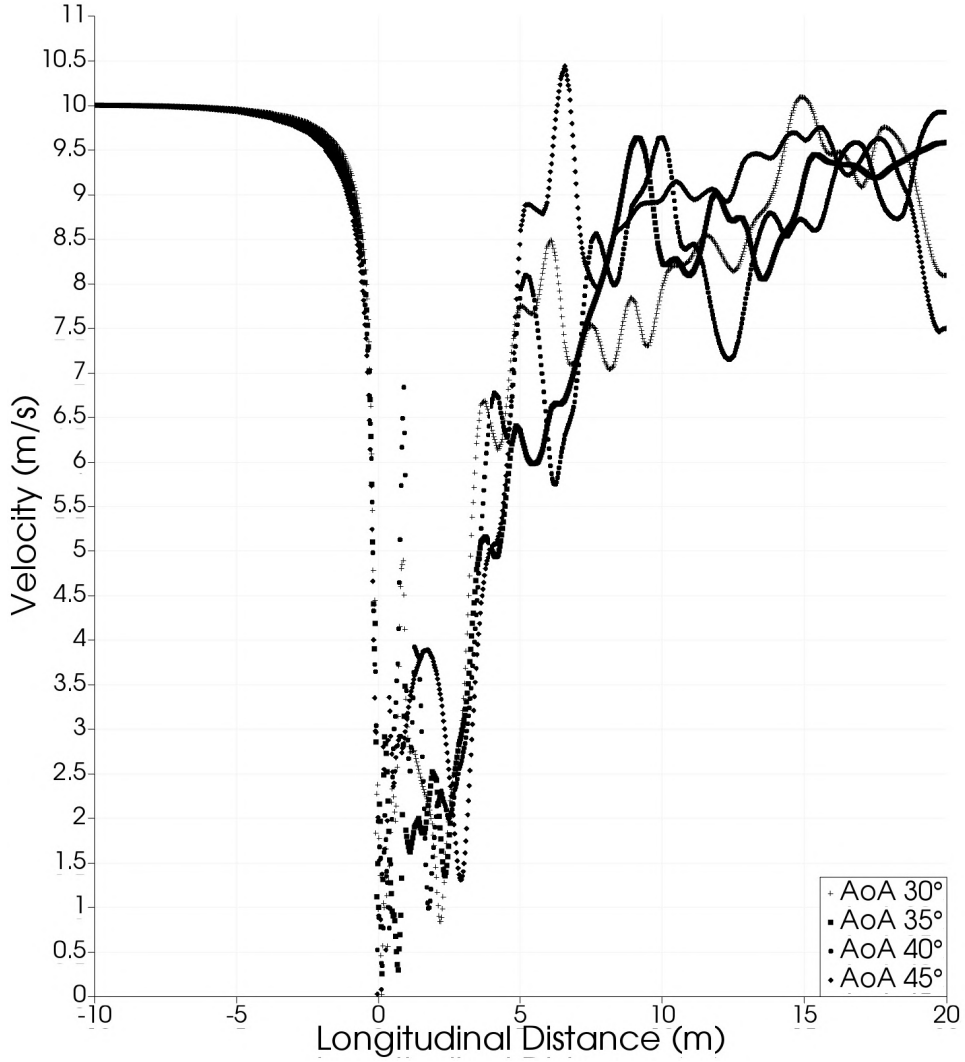

Figure 8: Longitudinal velocity recovery for different angles of attack from 30°to 45°

respectively. Presenting iso-values of the vorticity magnitude in 2D. As expected the greater the angle of attack the bigger are the eddy structures presented in the downstream wake of the NREL S809. Therefore, qualitative analyses of vorticity it is important to gather knowledge to specified the better refinement criteria around this parameter, in order to have lower computational cost with better accuracy and physical representativeness.

6. CONCLUSION

A great evaluation analysis of wind resources and parameters is required to gather excellent performance of the wind power. Thus, the main goal of this study was to access how large eddy simulation alongside immersed boundary method behaviors, in order to characterize the most important parameters experimental wind turbine blade aerodynamics. The experimental wind turbine blade utilized was the NREL S809, with the inflow wind speed set to be 10 m/s.

The drag and lift coefficients results showed good agreement in comparison to the experimental data from NREL, in function of different angles of attack. The drag coefficient itself presented excellent results for all the angles ranges up to 35°. However, it can be improved the agreement of the lift coefficients, if the increment of the angle of attack decreases for 1°or 2°, in the 0 to 15°region. The ratio C_l/C_d showed high ratios of performance in the small angles, which is closer to the stalling angle.

In terms of velocity recovery, the downstream wake centerline velocity recovery analysis for different angles of attack presented a quick recovery for small angles of attack up to 70% for $x = 1D$, reaching 85% to 90% of the initial free stream wind speed at the end of the domain. However, for greater angles of attack, the recovery was a bit slower reaching 65% at $x = 1D$, but achieving almost 100% recovery at the end of the domain for a couple of angles. By the end, a qualitative vorticity evaluation of how the eddies structures increases as the angle of attack gets bigger as expected, presenting in snapshots the iso-values of the vorticity magnitude.

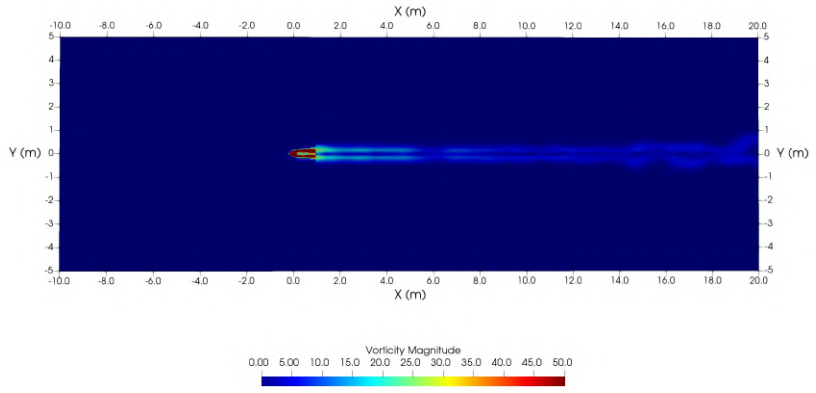

(a) 10°

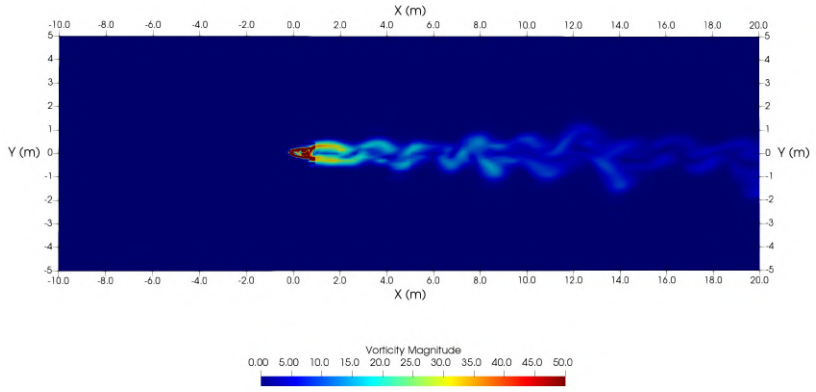

(b) 20°

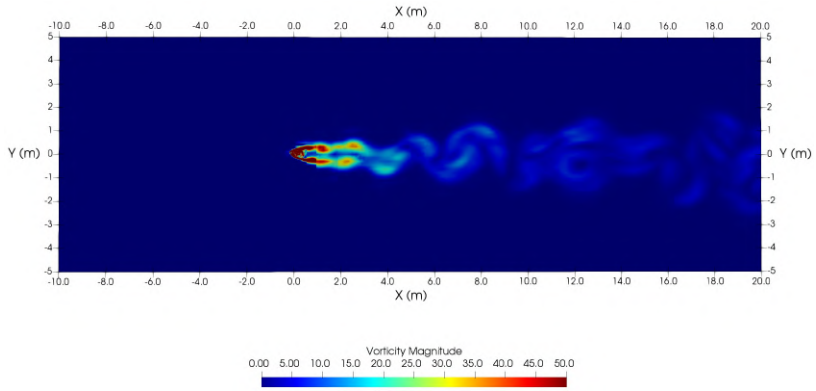

(c) 30°

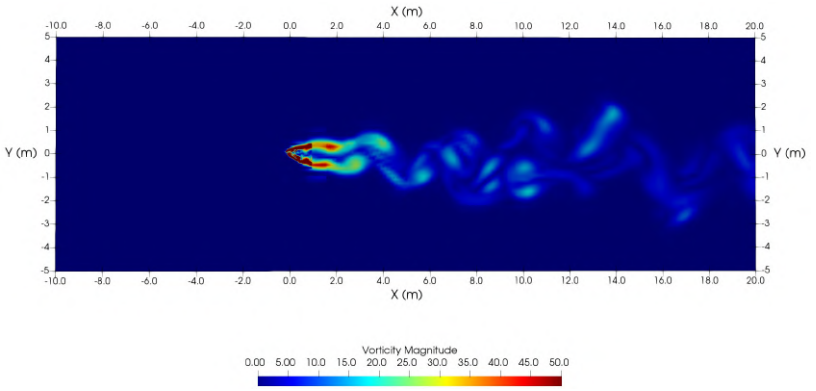

(d) 40°

Figure 9: Vorticity for different angles of attack, from (a) 10°, (b) 20°, (c) 30°and (d) 40°

7. REFERENCES

Barbi, F., 2016. *Experimentação numérica de bolhas em ascensão*. Ph.D. thesis, Universidade Federal de Uberlândia, Uberlândia, Brasil.

Çengel, Y., 2010. *Fluid Mechanics*. Çengel series in engineering thermal-fluid sciences. Tata McGraw Hill Education Private. ISBN 9780070700345. URL https://books.google.com.br/books?id=c8ATbn9ChB8C.

da Silva Melo, R.R., 2012. *Formulações Integral e Diferencial Aplicadas à Análise de Escoamentos Sobre Rotores Eólicos*. Master's thesis, Universidade Federal de Uberlândia, Uberlândia.

Edelenbosch, O., Kermeli, K., Crijns-Graus, W., Worrell, E., Bibas, R., Fais, B., Fujimori, S., Kyle, P., Sano, F. and van Vuuren, D., 2017. "Comparing projections of industrial energy demand and greenhouse gas emissions in long-term energy models". *Energy*, Vol. 122, pp. 701 – 710. ISSN 0360-5442. doi:https://doi.org/10.1016/j.energy.2017.01.017. URL http://www.sciencedirect.com/science/article/pii/S0360544217300178.

Hand, M.M., Simms, D.A., Fingersh, L.J., Jager, D.W., Cotrell, J.R., Schreck, S. and Larwood, S.M., 2001. "Unsteady aerodynamics experiment phase vi: Wind tunnel test configurations and available data campaigns".

Leung, D. and Yang, Y., 2012. "Wind energy development and its environmental impact: A review". *Renewable and Sustainable Energy Reviews*, Vol. 16, pp. 1031–1039. doi:10.1016/j.rser.2011.09.024. URL https://www.sciencedirect.com/science/article/pii/S1364032111004746.

Lund, H., 2007. "Renewable energy strategies for sustainable development". *Energy*, Vol. 32, No. 6, pp. 912 – 919. ISSN 0360-5442. doi:https://doi.org/10.1016/j.energy.2006.10.017. URL http://www.sciencedirect.com/science/article/pii/S036054420600301X. Third Dubrovnik Conference on Sustainable Development of Energy, Water and Environment Systems.

Mehta, D., van Zuijlen, A., Koren, B., Holierhoek, J. and Bijl, H., 2014. "Large eddy simulation of wind farm aerodynamics: A review". *Journal of Wind Engineering and Industrial Aerodynamics*, Vol. 133, pp. 1 – 17. ISSN 0167-6105. doi:https://doi.org/10.1016/j.jweia.2014.07.002. URL http://www.sciencedirect.com/science/article/pii/S0167610514001391.

Mittal, R. and Iaccarino, G., 2005. "Immersed boundary methods". *Annual Review of Fluid Mechanics*, Vol. 37, No. 1, pp. 239–261.

Mo, J., Choudhry, A., Arjomandi, M., Kelso, R. and Lee, Y., 2013. "Effects of wind speed changes on wake instability of a wind turbine in a virtual wind tunnel using large eddy simulation". *Journal of Wind Engineering and Industrial Aerodynamics*, Vol. 117, pp. 38–56.

Ramsay, R., Hoffman, M. and Gregorek, G., 1995. "Effects of grit roughness and pitch oscillations on the s809 airfoil".

Rehman, S. and Al-Abbadi, N.M., 2005. "Wind shear coefficients and their effect on energy production". *Energy Conversion and Management*, Vol. 46, pp. 2578–2591.

Sanderse, B., 2009. "Aerodynamics of wind turbine wakes literature review".

Simms, D., Schreck, S., Hand, M. and Fingersh, L., 2001. "Nrel unsteady aerodynamics experiment in the nasa-ames wind tunnel: A comparison of predictions to measurements".

Snel, H., 2003. "Review of aerodynamics for wind turbines". *Wind Energy*, Vol. 6, No. 3, pp. 203–211.

Tsalicoglou, C., 2012. *Numerical Study of Wind Turbine Wake Aerodynamics in Uniform and Yawed Inflow*. Master's thesis, Swiss Federal Institute of Technology, Swiss.

Vermeer, L., Sørensen, J. and Crespo, A., 2003. "Wind turbine wake aerodynamics". *Progress in Aerospace Sciences*, Vol. 39, p. 467–510.

Wang, Z., Fan, J. and Luo, K., 2008. "Combined multi-direct forcing and immersed boundary method for simulating flows with moving particles". *International Journal of Multiphase Flow - INT J MULTIPHASE FLOW*, Vol. 34, pp. 283–302.

Wharton, S. and Lundquist, J.K., 2012. "Atmospheric stability affects wind turbine power collection". *Environmental Research Letters*, Vol. 7.

Zhong, W., An, H., Shen, L., Dai, T., Fang, W., Gao, X. and Dong, D., 2017. "Global pattern of the international fossil fuel trade: The evolution of communities". *Energy*, Vol. 123, pp. 260 – 270. ISSN 0360-5442. doi:https://doi.org/10.1016/j.energy.2017.02.033. URL http://www.sciencedirect.com/science/article/pii/S0360544217302074.

Şiir Kılkış, Krajačić, G., Duić, N., Rosen, M.A. and Al-Nimr, M.A., 2018. "Advancements in sustainable development of energy, water and environment systems". *Energy Conversion and Management*, Vol. 176, pp. 164 – 183. ISSN 0196-8904. doi:https://doi.org/10.1016/j.enconman.2018.09.015. URL http://www.sciencedirect.com/science/article/pii/S0196890418310100.

8. RESPONSIBILITY NOTICE

The authors are the only responsible for the printed material included in this paper.